Chris Händel • Timo Saarenpää & Matti Autioniemi

B

Detecting Passive Radar Reflectors for Automotive Applications

Aurora Arctic Challenge Mobile Road Tests 2018/19 on Muonio Intelligent Road

PUBLICATIONS OF LAPLAND UNIVERSITY OF APPLIED SCIENCES
Series B. Research reports and compilations. 23/2019

Detecting Passive Radar Reflectors for Automotive Applications

Dr. Chris Händel, Timo Saarenpää and Matti Autioniemi

Detecting Passive Radar Reflectors for Automotive Applications

Aurora Arctic Challenge Mobile Road Tests 2018/19 on Muonio Intelligent Road

Series B. Research reports and compilations. 23/2019

Lapland University of Applied Sciences
Rovaniemi 2019

ISBN 978-952-316-326-3 (nid.)
ISSN 2489-2629 (painettu)
ISBN 978-952-316-327-0 (pdf)
ISSN 2489-2637 (verkkojulkaisu)

Publications of Lapland University of Applied Sciences
Series B. Research reports and compilations.
23/2019

Financiers: Aurora, Co Financed by the European Union - Connecting Europe Facility,
Traficom - Finnish Transport and Communications Agency, Väylä - Finnish Trasport Infrastucture Agency
Writers: Chris Händel, Timo Saarenpää and Matti Autioniemi
Layout: Lapland UAS, Communications

Lapland University of Applied Sciences
Jokiväylä 11 C
96300 Rovaniemi

Phone. 020 798 6000
www.lapinamk.fi/publications

The Lapland University Consortium (LUC) is a strategic alliance between the University of Lapland and Lapland Univeristy of Applied Sciences.
www.luc.fi

Content

1. Introduction

Road traffic is becoming more and more digital, automated and connected [1]. Some automated cars, such as the self-driving vehicle from Google, are already operating on public roads or are in the developing and testing phase [2]. The automation of these vehicles is mostly based on sensors (e.g. radars, Lidars, GPS and cameras) detecting their surroundings and environment [3, 4].

Despite the importance of automated vehicles to the future of road transport in the whole world, most of the field tests were carried out under ice- and snow-free weather conditions. Harsh winter conditions especially cause numerous challenges for automated cars and their sensors. Snowstorms, for example, blind cameras and magnetic storms can cause major difficulties for GPS systems [5]. Furthermore, obscured lane markings are a problem for automated vehicles especially in the northern countries.

Radar systems can operate in these harsh weather conditions. The emitted radar waves can penetrate rain, dust, fog and snow, making those systems indispensable for current technologies supporting automated vehicles (e.g. ACC). Strong reflecting objects along the roadside could support the navigation of vehicles using high frequency (76-81 GHz) radars. [6]

The present publication is the third and final part of a report series focussing on automotive radar systems, and passive radar reflectors. Both are one milestone in the Arctic Challenge research project and will be studied with regard to cold and icy outer conditions. This third part is a continuation to the State-of-the-Art Review on Automotive Radars and Passive Radar Reflectors that was published in May 2018 [7] and a report Detecting Passive Radar Reflectors for Automotive Applications that was published in May 2019 [8] in the publication series of research reports and compilations of the Lapland University of Applied Sciences Ltd. (Lapland UAS). All three reports deal with the following research questions:

1. What landmarks, such as delineators and reflective posts, or snow poles and plot access marks, support automated driving?
2. Where should these be located?
3. What should they be like?
4. How do different commercial passive radar corner reflectors compare in terms of reflective properties for an automotive application?

5. What is the effect of snow on the performance of a passive corner radar reflector?
6. What is the influence of typical roadside furniture on radar signals?

The present report summarizes the field tests, that were carried out in Rovaniemi (Finland) during the winter 2017/18. The report describes further the development of self-designed tubular reflector poles and their practical field tests in Muonio during the winter period 2018/19. In chapter 2, the basics of radar techniques, passive radar reflectors and laser scanning are introduced. In chapter 3, relevant information concerning the applied methods and the equipment used are given. In this chapter the test areas in Rovaniemi and Muonio, the applied radar systems, the tested passive radar reflectors, the test vehicle and the test plan are introduced to the reader. In chapter 4, the results of the measurements are presented and discussed concerning the earlier mentioned research questions. The first part of the chapter summarizes the practical field tests carried out in Rovaniemi during the winter period 2017/18. The second part focusses on field tests carried out in Muonio during the winter period 2018/19. In chapter 5, the results and conclusions of the report are summarized and some ideas and recommendations for future steps are given.

2. Background

2.1 RADAR TECHNIQUES

The weak interaction with falling snow, dust and rain make radio waves (3 MHz – 110 GHz) a suitable tool to perform measurements under challenging weather conditions [9, 10]. Based on its properties, radar waves are applied, among other things, in earth science (e.g. GPR) and in the automobile industry (e.g. ACC). [8, 11].

Typically, a radar setup consists of a transmitter generating radar waves [12] and a transmitting antenna (TX) sending the waves as primary signal in the space. The emitted signal can be scattered and reflected by a target [11, 13]. A receiver (RX) detects the reflected signal after a time Δt. (see **Figure 1a**).

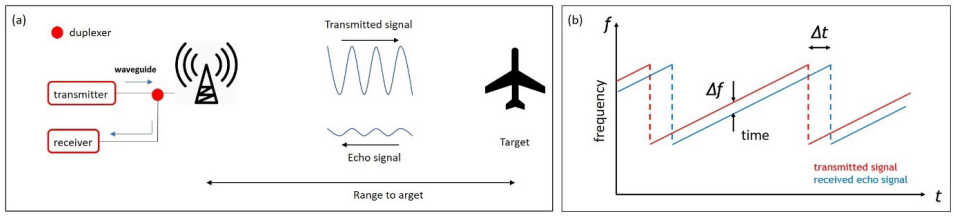

Figure 1: Principle setup of a radar system and principle of FMCW radars. (a) Radar setup containing a transmitter, an antenna, a duplexer and a receiver [8]. (b) Working principle of FMCW radars sketched in a frequency-time graph [8].

Depending on the sent signal, radar systems can be classified as pulsed and continuous wave (CW) systems. Pulsed systems sent µs-pulses and receive the reflected pulse after a time Δt. The distance R to the target can be estimated from the runtime Δt of the sent pulse to the target and back [12]:

$$R = \frac{c \cdot \Delta t}{2}. \tag{1}$$

Contrary to pulse radars, continuous wave systems emit quasi-continuous waves. The distance R between the radar and the target can be calculated by applying periodically frequency modulated (FMCW) radar waves. A frequently used modulation is the sawtooth pattern (see **Figure 1b**). A more detailed discussion of the working principle of FMCW radars is given in [8].

2.2 REFLECTOR TECHNIQUES

Radar reflectors are developed to optimally reflect radar radiation. They can be applied to mark poorly reflecting targets. A physical property, characterizing the efficiency of radar reflectors, is the radar cross section (RCS) [10]. The RCS is generally defined as:

$$\sigma = 4\pi R^2 \frac{P_{scat}}{P_{em}}. \tag{2}$$

P_{scat} is the scattered power density at a distance R from the reflector and P_{em} is the power density of the radiation at the reflectors position. The RCS of a radar reflector is material property and depends on the properties of the incoming radiation and the reflectors geometry as well. [10]

Radar reflectors are often based on the principle of retro-reflection. Retro-reflection is the reflection of incoming radiation independently from the reflectors' orientation (see **Figure 2a**). Retro-reflection can be realized via corner reflectors. Especially metallic corner reflectors have good reflecting characteristics for radar radiation while corner reflectors made of glass prisms are mainly applied for Lidars. Usual corner reflectors consist of three plane, mutually perpendicular and conductive surfaces that can reflect a radar wave up to three times (see **Figure 2b**). [14]

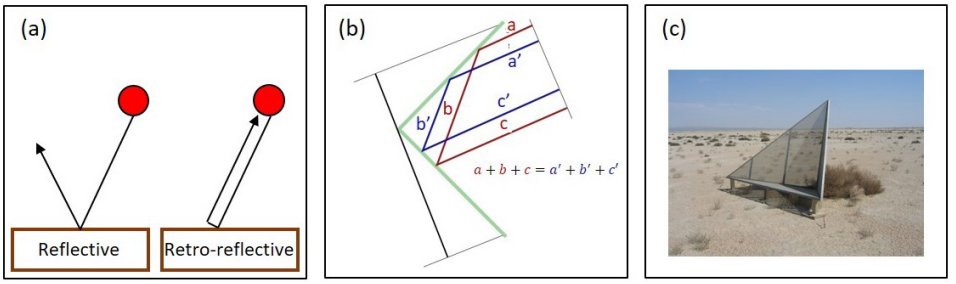

Figure 2: Corner reflectors. (a) The principle of retro-reflection. The incoming electromagnetic wave is reflected along a parallel vector to the radar emitting antenna (red dots). Adapted from [15]. (b) Working principle of a corner reflector [8, 16]. (c) A triangular corner reflector (Rosamond Calibration Array). The surfaces are attached to each other at the edges forming a corner [17].

The radar cross-section can be calculated for trihedral (see **Figure 2c**) and cubic corner reflectors using [18, 19]:

$$\sigma_{tr} = \frac{4\pi a^4}{3\lambda^2} \qquad \sigma_{cub} = \frac{12\pi a^4}{\lambda^2}. \tag{3}$$

a is the edge length and λ the wavelength of the radiation ($\lambda \ll a$). A deeper discussion of the RCS as well as retro-reflection is given in [8].

2.3 LASER SCANNING

Scanning surfaces with laser light, to produce an image of it, is called laser scanning. In analogy to radar, the distance R between target and laser can be calculated from the runtime Δt of the emitted Laser signal to the target and back. Due to its physical properties, laser scanning is an ideal tool to analyse roads and roadside furniture. With a known laser beam angle and an exact vehicle position, a 3D surface image, or "point cloud", from the road and its surroundings can be reconstructed. The accuracy of the laser scanner surveys is limited by factors reducing visibility, such as dust, rain, fog or snow.

A laser scanner consists of a laser cannon, a scanner and a detector. The laser cannon produces the laser beam, the scanner circulates the laser beam, and the detector measures the reflected signal and defines the distance to the target. More detailed information concerning laser scanning is provided in [20].

3. Materials and Methods

3.1 TEST FIELD, OUTER CONDITIONS AND TEST PREPARATION

All tests were performed on test tracks to provide comparable experimental conditions between different tests. One is located near the airport of Rovaniemi and one in Muonio on a ≈10 km instrumented road section on Finnish national road 21, which is part of the European route E8 (Aurora Intelligent Road). The first mentioned test field is 25 m and wide 165 m long, (**Figure 3a** and **3b**). For the tests in Muonio, a ≈1.5 km long road section was selected from the Aurora Intelligent Road and prepared with 100 reflector mounting poles on top of which the actual reflector tubes were installed before the test period (**Figure 3c**). The section includes in total 189 holders for reflector mounting poles (20 m distance, respectively) on the left and right side of the road (**Figure 4a** and **4b**). The distance between reflector pole holders and road was always 3 m during the tests. Holders with a smaller distance to the road were not chosen to avoid problems with the winter road maintenance. All experiments were performed under winter conditions (**Figure 4c**). The radar enclosure height was 60 cm above the ground in both test tracks. The test period was between 4.3. and 8.3.2019 and before that the reflectors were assembled and installed inside the reflector tubes. The road safety planning and the necessary road safety announcements were made in cooperation with authorities before the test period. On the first test day, the reflector tubes were mounted on top of the reflector poles and the necessary road safety measures were taken.

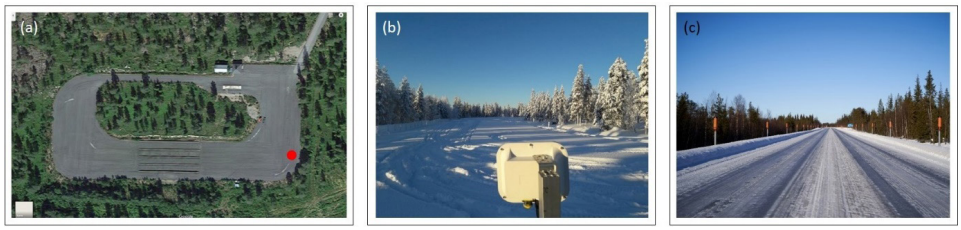

Figure 3: Test fields in Rovaniemi and Muonio. (a) Photograph of the test field in Rovaniemi (66°32'52"N 25°48'36"E) [21]. The red dot shows the position of the radars. [8] (b) Test track in winter 2018 before a measurement. [8] (c) Test section on E12/Vt21 in Muonio. On the left and right side are reflector poles.

(c)

Location	Temperature	Snow high	Ground
Rovaniemi	-15 °C	> 1 m	rough, slope
Muonio	-10° C	≈ 25 cm	flat

Figure 4: Test field in Muonio. (a) A representative empty foundation for a reflector pole (concrete holder, grey). (b) The selected road section in Muonio including 189 pole holders. The red coloured dots show empty holders while the green coloured dots show reflector locations. (c) Overview of conditions at the test tracks.

3.2 APPLIED RADAR SYSTEM - ARS 408-21 FROM CONTINENTAL AG

Continental's premium radar sensor 408-21 is designed for automotive applications. The sensor operates with a dual scan (serially alternating) and 77 GHz. The dual scan facilitates switching between short- and far-range mode (see **Figure 5**). The radar sensor further contains multiple antennas for simultaneous detection of targets. [8]

In order to protect the sensor from moisture, the radar was enclosed with a plastic box. In mobile measurements, the plastic box was further equipped with a holder to fix it in front of the test vehicle. Prior to an experiment, the radar was connected to a CAN (Controller Area Network) module providing the communication between the radar and the computer. A PLC (Programmable logic controller) was used to display the collected data on a screen. [8]

The ARS 408-21 radar is based on FMCW modulations realizing an independent velocity and distance monitoring of objects in one measurement cycle. The objects' information is calculated in every cycle and the position is displayed in a coordinate system relative to the radar sensor. A technical description of the radar sensor is given in [22]. [8]

Besides the 408-21 Premium sensor from Continental, two other radar systems from Furuno Electric Co., Ltd. and Texas Instruments Inc. (TI) were tested regarding accuracy, resolution, data output and handling [8]. All three radars are suitable for transport applications.

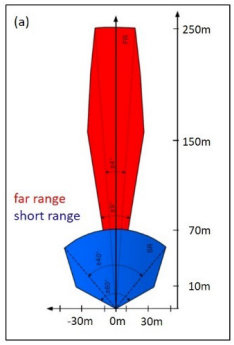

(b)

Distance range	0.20 ... 250 m far range, 0.20 ... 70m/100m@0...±45° near range, 0.20 ... 20m@±60° near range
Resolution distance measuring	1.79 m far range, 0.39 m near range
Accuracy distance measuring	±0.40 m far range, ±0.10 m near range
Azimuth angle augmentation	-9.0°...+9.0° far range, -60°...+60° near range
Elevation angle augmentation	14° far range, 20° near range
Resolution azimuth angle	1.6° far range, 3.2°@0° / 4.5°@±45° / 12.3°@±60° near range
Accuracy azimuth angle	±0.1° far range, ±0.3°@0°/ ±1°@±45°/ ±5°@±60°near range

Figure 5: ARS 408-21 radar sensor. (a) The digital antenna offers two independent scans for far and short range. The sensor contains 2 TX and 6 RX antennas for near range and 2 TX and 6 RX antennas for far range scan using digital formed beams. [8, 23] (b) Selected information from the datasheet. [23]

3.3 APPLIED RADAR REFLECTORS

3.3.1 Commercially Used Radar Reflectors

Commercially applied corner reflectors are often made of anodized aluminium. These reflectors are typically octahedral shaped or perpendicular stacked dihedrals. Octahedral radar reflectors are commonly diamond-shaped or built from circular panels slotted together. [8, 24]

For the later described experiments, four radar reflectors from the maritime sector were selected and acquired. The chosen models are shown in **Figure 6**. The first and the third reflector are octahedral shaped and have a diameter of ≈40 cm. Both consist of aluminium panels which are locked in place by plastic corners. The second reflector is a tubular reflector. The model consists of longitudinal arranged dihedrals in a transparent plastic cover. The fourth tested model is the Echomax EM180. It is vertical stack of three aluminium corner arrays enclosed in a plastic cover. The results and conclusions of a performance investigation of the reflectors are presented in [25].

Figure 6: Radar reflectors used in the maritime sector. Presented is a selection of four radar reflectors used in the maritime sector. [8]

3.3.2 Self-designed Corner Reflectors

In order to develop more practicable, cheaper and fast to produce radar reflectors, Lapland UAS designed and acquired four different octahedral corner reflectors. The principle of the self-designed corner reflectors is shown in **Figure 7a**. The design is similar to the octahedral, circular 40 cm reflector introduced in **chapter 3.3.1**. Designed were extra-large (Ø 20 cm), large (Ø 10 cm), medium (Ø 4.05 cm) and small (Ø 1.649 cm) prototypes made from aluminium (10 respectively, **Figure 7b**). For some preliminarily experiments, the reflectors were fixed on plastic poles (**Figure 7c**).

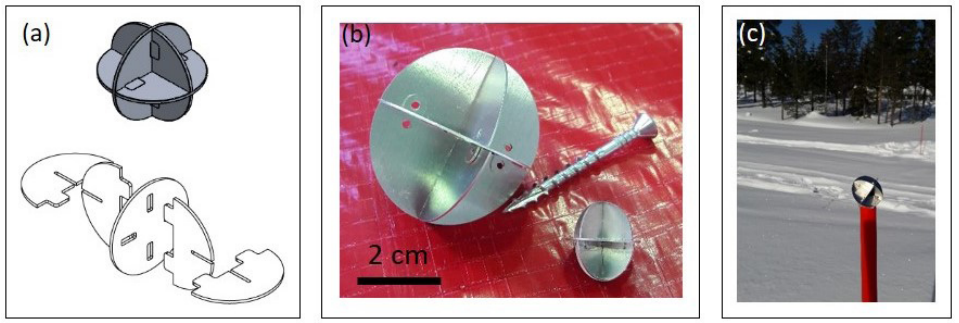

Figure 7: Self-designed aluminium radar reflectors. (a) Sketch and design drawing of the self-designed corner reflectors. [8] (b) Medium (left) and small (right) self-designed corner reflector. Shown is one prototype respectively. [8] (c) Self-designed corner reflector (medium version) on top of a plastic pole (60 cm high). [8]

3.3.3 Self-designed Tubular Reflector Poles

Based on the tested reflectors shown in the **chapters 3.3.1** and **3.3.2**, a tubular reflector pole was developed. It consists of a plastic pipe and an enclosure containing three Ø20 cm corner reflectors (**Figure 8a**). The three reflectors can be rotated against each other and positioned along the same axis in the tube to optimize the visibility. A plastic cover protects the single reflector plates from falling snow. The reflector design was developed according to our previous results indicating that snow covered reflector plates negatively affect the reflectors' visibility [8]. The pole height of ≈ 1.8 m above the ground was chosen to avoid the reflector being covered by snow. A selection of the self-designed tubular reflector poles in the test field in Muonio is shown in **Figure 8b**. Altogether, 100 tubular reflector poles were manufactured and 97 of them were installed on the left and right side of the road. **Figure 8c** illustrates the experimental setup in Muonio.

Before the actual test period, pre-testing was conducted during January 2019 in Rovaniemi with 10 complete prototype reflector poles. For the pre-testing, the Continental radar was mounted on the front bumper of the test vehicle. The pre-tests were measured with a driving speed of 30km/h and the results showed the reflectors were clearly visible for the radar. Based on this positive result, the remainder of 90 reflector tubes was ordered.

Figure 8: Self-designed reflector poles. (a) Self-designed tubular reflector pole containing three Ø20 cm corner reflectors. A plastic cover (brown) protects the single reflector plates from falling snow. (b) Photograph of the experimental setup in the test field in Muonio. The longitudinal distance between the reflectors is 20 m respectively (in one section 40 m). (c) Sketch of the experimental setup in Muonio. Shown is the position of the radar (yellow) on the road. The red dots on the left and right side illustrate ten representative reflector poles.

3.4 THE TEST VEHICLE

The measurements on the test track in Muonio were carried out with the Road Doctor Survey Van (RDSV). The RDSV is a non-destructive survey system designed for road condition data collection and analysis. In our tests the RDSV was equipped with the RD CamLink-system, the RD Laser Scanner with a 3D accelerometer, IMU capable GPS and the ARS 408-21 radar sensor from Continental (**Figure 9a**).

The RD CamLink-system is designed to collect videos, audio commentary and drainage or pavement distress inventory on the road, together with GPS coordinates. The main components of the RD CamLink-system are two (out of a possible three) GigE connected industrial colour cameras (up to 30 images per second) protected by enclosures (**Figure 9b**), a GPS device and a laptop. The video can be directly digitized and stored at 1280*960 pixels. Both cameras were fixed with a mounting system on the roof of the RDSV. Location information could be collected simultaneously with other survey data using the Road Doctor® CamLink program with GPS and DMI (accuracy better than 0.1 m). The collected location information is then used to update the road network and it can be transferred into any GIS, capable of reading ESRI shape files. The software has built-in support for GPS (WGS84) coordinate transformations to any location referencing system. The original road network location information can be imported into the Road Doctor® software and further used to navigate to the desired location. It was also used to check and validate the data positioning quality.

In addition to the radar and camera system, the data collection was carried out using a SICK LMS511 laser scanner (**Figure 9c**). The laser scanner was mounted at the back of the survey van. Based on the laser scanning data, a 3D profile of the road and the surroundings can be produced, and the position of the radar reflector poles can be displayed on a map. The scanning range is up to 65 m. The laser scanner data was

measured simultaneously with an 3D accelerometer, GPS and digital image data using RD CamLink.

The Road Doctor® software was used in the field data collection, data processing and analysis. This software facilitates integrated analysis of the laser scanner data together with videos and maps. The software has been developed by Roadscanners Oy.

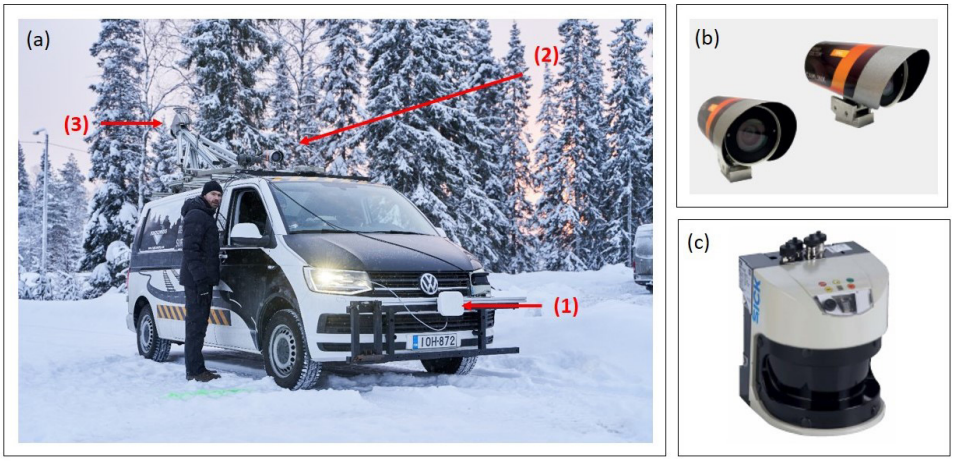

Figure 9: Road Doctor Survey Van. (a) Road Doctor Survey Van in a field test. The Van is equipped with (1) the ARS 408-21 radar sensor from Continental, (2) the RD CamLink - system and, (3) the SICK LMS511 laser scanner in a close-up. (b) GigE connected industrial colour cameras. (c) SICK LMS511 laser scanner.

Test Number	Direction	Speed [km h^{-1}]	Poles	Comments
1	1	30	no	few cars
2	2	30	no	few cars
3	1	60	no	no cars
4	2	60	no	no cars
5	1	80	no	truck outside track
6	2	80	no	few cars
7	1	30	yes	few cars
8	2	30	yes	no cars
9	1	60	yes	two cars passed by
10	2	60	yes	no cars
11	1	80	yes	few cars

Test Number	Direction	Speed [km h^{-1}]	Poles	Comments
12	2	80	yes	no cars
13	1	80	yes	Right side of the lane, one car
14	2	80	yes	Right side of the lane, one car
15	1	80	yes	Left side of the lane, no cars
16	2	80	yes	Left side of the lane, no cars
17	1	80	yes	zig zag, few cars
18	2	80	yes	zig zag, no cars
19	2	80	yes	behind a car
20	1	80	yes	car passing by
21	2	80	yes	blow snow
22	2	80	yes	behind a truck

Figure 10: Test plan from the test track in Muonio.

3.5 THE TEST PLAN

For the experiments on the test track in Muonio (**Figure 4b**) a test plan was developed (**Figure 10**). Results of pre-testing and knowledge gained from previous field tests were utilized to find different test scenarios for the mobile road tests in Muonio. The objective was to define several test scenarios which would mimic real situations that occur in everyday traffic. The plan contains tests at different speeds (30, 60 and 80 km/h) and in different directions. "Direction 1" stands for driving towards Muonio (from south to north) and "direction 2" means driving away from Muonio (from north to south). Test plan described in the **Figure 10** gives an overview of the defined scenarios.

4. Results and Discussion

In the present chapters, the test results from several radar and reflector experiments are presented and discussed. The experiments were prepared and conducted as introduced in **chapter 3.1**. The first part gives a summary of the practical field tests carried out in Rovaniemi during the winter period 2017/18. These tests should determine which radar system and which radar reflector type is most suitable for further field tests on a road. All test cases were developed concerning the research questions formulated in the introduction. Based on these results, a tubular reflector pole was designed and an experimental setup on a road was developed. The results presented in **chapter 4.1** are published in [8]. The second part describes field tests carried out in Muonio during the winter period 2018/19. Studying the self-designed reflector pole on a road was the focus of these experiments.

4.1 SUMMARY OF THE FIELD TESTS PERFORMED IN 2017/18

The practical tests of this field study were carried out on the test track in Rovaniemi (**Figure 3a** and **9b**) during the winter period 2017/18. All presented results were published and discussed in the publication series of research reports and compilations of the Lapland University of Applied Sciences Ltd. (Lapland UAS) [8].

Tested were three radar systems suitable for transport applications: The system from Continental AG, Furuno Electric Co., Ltd. and Texas Instruments Inc. (TI). In **chapter 4.1.1** the test field background and the impact of human presence on the radar signal were investigated to estimate their influence on further experiments. In **chapter 4.1.2**, different types of passive radar reflectors (commercially used and self-designed) in different form and size were tested regarding their practicability, reflectivity (RCS) and detectability for our applications. Based on these preliminary results, a mobile test was developed and carried out (**chapter 4.1.3**). This mobile test provides the basis for further tests in Muonio during the winter 2018/19. Finally, the influence of roadside furniture and snow on the radar signal was investigated in **chapter 4.1.4**.

4.1.1. Test Field Background and the Influence of Human Presence on the Radar Signal

First, reference measurements were conducted with each radar. The characterization of typical objects in the surroundings concerning their RCS was the aim of these tests. In these experiments the test field only, without humans or equipment, was monitored (61 s, 136 data point/10 s). The experimental results show that, the test field is free from reflecting objects with $\sigma < 16$ m². It is concluded that 16 m² is an adequate threshold for the detectability of objects in further experiments. The test field background measured with the radars from Continental, TI and Furuno are shown in [8].

Further, the impact of humans on the radar signal was investigated with the three radars. In these tests a human, dressed in winter clothes, walked in the test track. Other reflectors were not present during the experiment. Humans could not be detected, neither stationary nor walking, with the selected noise level of $\sigma = 16$ m². The results are summarized in **Figure 11**. The described results lead to the conclusion, that pedestrians will not remarkably influence the tests, performed with the chosen setup. [8]

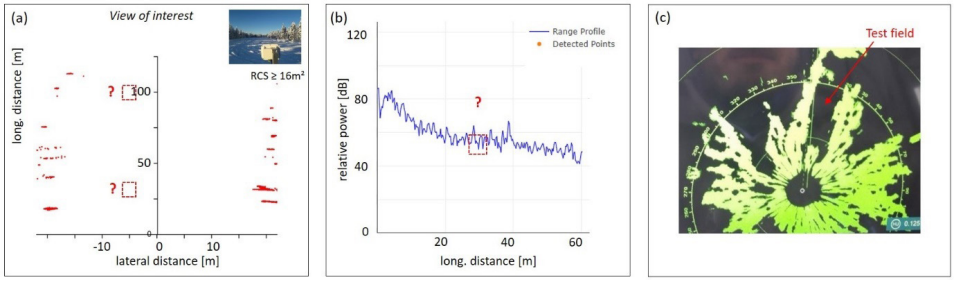

Figure 11: Test Field Background and the Influence of Human presence.
(a) Longitudinal - lateral distance graph of the test track measured with the ARS 408-21 sensor from Continental. The graph shows only reflections (red dots) with RCS of 16 m² or higher. On the left and right edge of the test field, multiple strong reflections are visible. These reflections are caused, among other things, by big trees and wires in the test track's surroundings. The red boxes in the centre of the plot show two positions where a human stood during the measurement (64 s). [8] (b) Range profile detected with the radar from TI. The position of the human is marked with a red box. [8] (c) Display screenshot of the NavNet TZtouch2 (Furuno) during an experiment. The black rectangle shows the test field with the surrounding area. [8]

4.1.2 Radar and Reflector Tests

In the present chapter the test results from radar measurements of different radar reflectors are summarized and discussed.

First, the octahedral, circular 40 cm reflector (**Figure 12a**) was monitored with the ARS 408-21 from Continental on different longitudinal positions (**Figure 12b**). Each position was measured (60 s) in a separate test. The reflections are displayed as red points and their RCSs range from σ (80 m) = (18 ± 3) m² to σ (60 m) = (794 ± 113) m². This deviation is based on the RCS' angle dependency. The detected accuracy is ± 0.2

m in lateral and ± 0.1 m in longitudinal direction [8]. Besides the octahedral, circular 40 cm reflector, three other reflectors (described in **chapter 3.3.1**) were analysed regarding detectability with the system from Continental. The test results are summarized in the upper table of **Figure 12c**. All four tested reflectors were also detectable with the radars from TI and Furuno. A detailed description of the experiments is shown in [8].

In a second experimental setup, the octahedral, circular 40 cm reflector was shifted in the test field. The test demonstrates that the corner reflector is quasi constantly detectable with the three radars, while it is moved (**Figure 13**). Further graphs are given in [8]. These positive results provide the basis for further tests involving a moving car. **Figure 13c** demonstrates the angle dependency of the RCS during the shift of the reflector. During the 100 s reflector shift, the RCS values fluctuate between around zero and 400 m². The result is in accordance with theoretical expectations introduced in **chapter 2.2**.

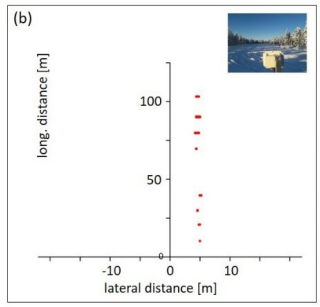

(c)

Longitudinal distance	Tubular reflector	Octahedral d.	Echomax EM180
20m	not detectable	26 ± 25 m² *	56 ± 28 m²
40m	not detectable	126 ± 1 m²	28 ± 2 m²
80m	not detectable	200 ± 16 m²	126 ± 1 m²
100m	not detectable	71 ± 61 m² *	116 ± 60 m²

Longitudinal distance	RCS [m²] Ø10 cm	RCS [m²] Ø20 cm
100m	*112/ 106*	*16/ 20*
80m	*9/ 9*	*200/ 186*
60m	*8/ 8*	*251/ 233*
40m	*9/ 9*	*79/ 169*
20m	*14/ 13*	*40/ 41*

Figure 12: Different radar reflectors tested with the 408-21 Sensor from Continental.(a) The octahedral, circular 40 cm reflector on a 60 cm high plastic pole while testing. [8] (b) Longitudinal-lateral distance plot measured with the Continental radar. The red dots show selected reflections caused by the octahedral, circular 40 cm reflector. Each reflection was measured in a separate experiment. [8] (c) Behaviour of different radar reflectors measured with the system from Continental. Each reflection was measured in a separate test. (upper table) Median RCS values (Median ± SD) measured in four different distances with the radar from Continental. (lower table) Self-designed reflectors tested with the Sensor from Continental. Median and mean RCS values measured in five different distances. [8]

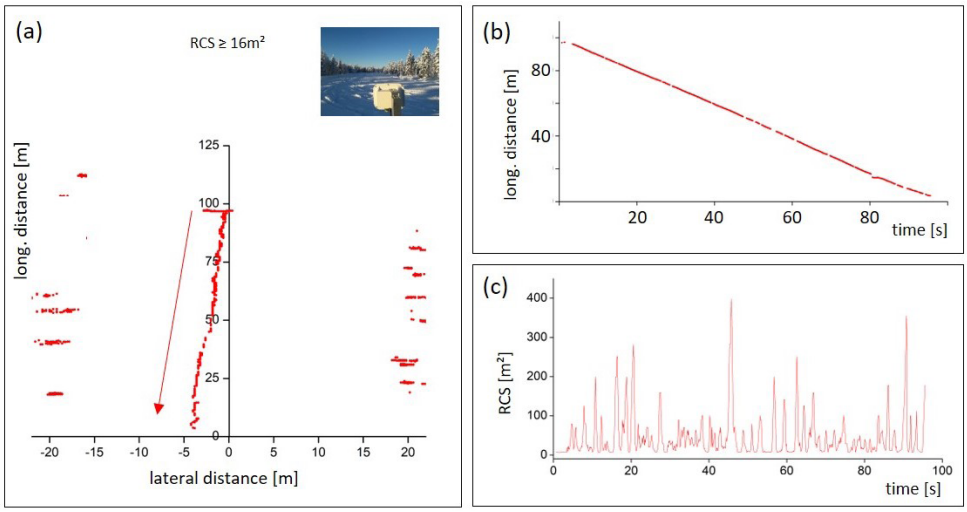

Figure 13: Shifted octahedral, circular 40 cm corner reflector measured with the radar from Continental. (a) Longitudinal-lateral distance plot. The reflector was moved from a position 100 m away from the radar towards the radar. The red arrow shows the direction of movement. [8] (b) Longitudinal distance-time plot. [8] (c) RCS-time plot. [8]

Beside the commercially used reflectors, four types of self-designed corner reflectors (**chapter 3.3.2**) were analyzed with the radar from Continental. The smaller (Ø 1.7 cm and Ø 4 cm) self-designed corner reflectors could not be detected at all. The RCSs of the self-designed Ø20 cm reflector and the octahedral, circular 40 cm reflector from the maritime sector are in the same order of magnitude (lower table in **Figure 12c**). Based on the results it is concluded, that our self-designed Ø20 cm reflectors are a cheap and fast-to-produce alternative, for our purposes, compared to current products on the market. [8]

4.1.3 Road-like Case and Mobile Tests Performed with the ARS 408-21 from Continental

The experiments described in the first part of this chapter build the basis for tests with a moving vehicle. The experimental setup (**Figure 16a** and **16b**) consisted of 10, self-designed Ø 20 cm reflectors (five on the left and five on the right side). The reflectors were attached on top of plastic poles. A longitudinal distance of 20 m between the poles was chosen based on the specifications of the radar from Continental (3 reflector poles per side are in the near range area of the radar) [23]. The location of the radar was chosen to be similar to that of a car on a road. The measured mean and median RCSs are given in the table in **Figure 16a**. [8]

For the mobile test, the same experimental setup as before was used. While testing, the radar from Continental was mounted on the front of a Van (see **Figure 9a**). **Figure 16c** shows the condition before the Van drove through the setup. The radar reflectors appear as points on the left and right side. The ten corner reflectors were simultaneously measured in one test. The vehicle's starting position was selected as sketched in **Figure 16a**. Ten seconds after the data collection had begun, the Van drove ($v \approx 6{,}5$ km/h)

through the setup. **Figure 16d** shows the time evolution of the lateral distance, during the measurement. The results show, that not all reflectors were detectable the whole time while the Van was driving though the test track. But at least five self-designed reflectors were always detectable and guaranteed an adequate tracking of the test road. Moreover, the tests show a strong angle dependency of the RCS for the individual reflectors (**Figure 16e**). [8]

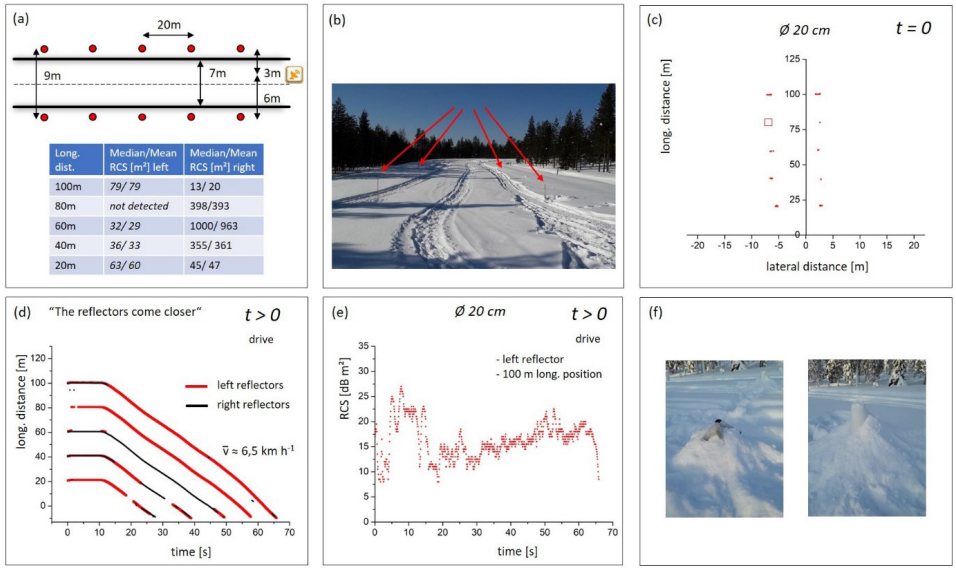

Figure 16: Self-designed radar reflectors in a road-like case and in a mobile test. [8] (a) (upper:) Setup sketch of the test field. The radar reflectors are located one meter away from the edge of the hypothetical road. The position of the radar is marked in yellow on the right side. (lower:) The ten radar reflectors were simultaneously measured in one test. (b) Photograph of the experimental setup. The arrows point towards the reflectors on top of plastic poles. (c) Longitudinal-lateral distance graph of the experimental setup before the Van started to drive. The measured radar reflections are shown as red dots. (d) Longitudinal distance-time graph for all 10 radar reflectors (simultaneously). The five reflectors on the left side are coloured in red and the reflectors on the right side in black. (e) RCS-time graph for a representative radar reflector while mobile measurement. (f) Selected test cases performed with the radar from Continental. The longitudinal distance between radar and reflector was 20 m (5 m lateral).

4.1.4 The Influence of Snow and Roadside Furniture on Radar Reflectors

In the present chapter, the influence of roadside furniture and snow on the radar signal is investigated. First, the four radar reflectors for maritime applications were positioned 20 m and 80 m (longitudinal direction) away from the sensor, in the test field. The reflectors were tested in separate experiments respectively. After positioning the test field was monitored (60 s) with radar sensors from TI and Continental. Subsequently, the radar reflectors were covered with snow incrementally and their detectability was observed. The results show, that dense packed snow had a strong effect on

the detectability of the tested reflectors. In contrast, moderate falling snow did not remarkably affect the detectability of the reflectors. **Figure 16f** shows some test cases conducted with the radar system from Continental. [8]

Further, a lamp pole and different metal poles were analyzed with the radars from Continental and TI. The lamp pole, as a typical representant of roadside furniture, could not be detected with all three radar systems. These experiments indicate that, typical roadside furniture, like lamp poles, are not practicable as reflectors for the applied radar instruments. Moreover, circular metal poles composed of different material were detected. All tested poles were not, or only weakly, detectable. The measured RCS is from one to two orders magnitudes smaller than some tested corner reflectors (e.g. Echomax EM180, σ (80 m) = (126 ± 1) m^2). It is concluded, that metal pipes are not practicable as radar reflectors for the applied radar systems. [8]

4.2 FIELD TESTS PERFORMED IN MUONIO 2019

All practical tests presented in this chapter were carried out on E12/Vt21 in Muonio (**Figure 3c** and **4**) during the winter period 2018/19. The test field in which the experiments were performed is described in **chapter 3.1**. The experiments discussed in this paragraph were carried out with our test vehicle (**chapter 3.4**) including the radar sensor from Continental, the RD CamLink-system as well as a laser scanner.

In **chapter 4.2.1** the test field background without reflector poles is discussed. The characterization of objects along the road, such as roadside furniture, is the prior goal of this measurement. The results of a test including 97 self-designed tubular reflector poles are presented in **chapter 4.2.2**. The test should clear up, if and how well the poles are detectable by radar at a driving speed of 80 km/h. The detected signal strength of the reflector poles will be compared to other objects along the road. **Chapter 4.2.3** focusses on the influence of driving speed on the positioning and the detected signal strength of the reflector poles. In **chapter 4.2.4** the effect of oncoming cars on the detectability of the reflector poles will be studied. Finally, the influence of blowing snow on the detectability and the positioning of the self-designed reflector poles will be discussed in **chapter 4.2.5**.

4.2.1 The Test Field Background without Reflector Poles

In order to obtain comparable starting conditions for further experiments, reference measurements were performed without reflector poles on the left and on the right side of the road. In these experiments the test section in Muonio was monitored by the radar and cameras while the vehicle (**chapter 3.4**) drove with different speeds through the test section. While measuring, the radar sensor from Continental was mounted on the front and the cameras on the roof of the vehicle. The characterization of typical objects in the surroundings and roadside furniture is an important goal of this measurement.

Figure 19a demonstrates a section of the 1.5 km long test field in Muonio without the reflector poles. The map shown in the figure is from the "National Land Survey of

Finland" WMS server. The surroundings of the road are characterized by multiple radar reflections (blue spots). These reflections are caused by, among other things, big trees and house roofs. The road itself is free of radar reflections. **Figure 19b – 19d** show different types of radar reflecting objects such as parked cars, snow poles and street signs. The detected signal strengths of the objects are summarized in **Figure 19e**. The measured values range from $\sigma = (11 \pm 0{,}7)\ m^2$ to $\sigma = (16 \pm 1{,}5)\ m^2$. Based on the results shown in chapters **4.1.2** and **4.1.3**, we expect significantly stronger signals backscattered from our self-designed reflector poles.

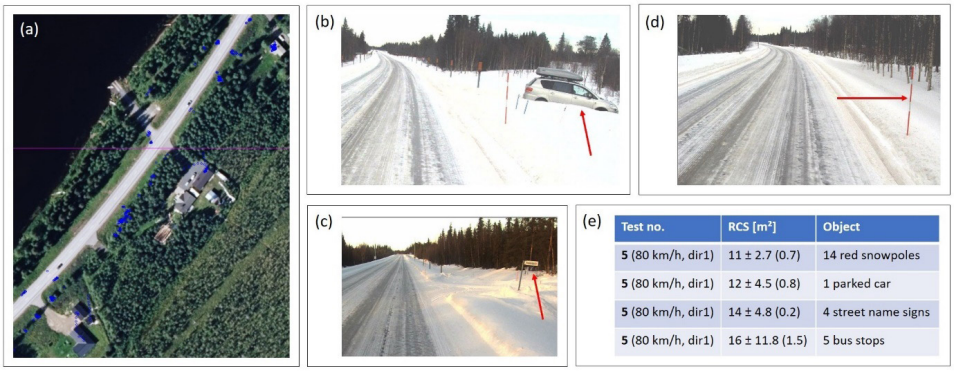

Test no.	RCS [m²]	Object
5 (80 km/h, dir1)	11 ± 2.7 (0.7)	14 red snowpoles
5 (80 km/h, dir1)	12 ± 4.5 (0.8)	1 parked car
5 (80 km/h, dir1)	14 ± 4.8 (0.2)	4 street name signs
5 (80 km/h, dir1)	16 ± 11.8 (1.5)	5 bus stops

Figure 15: Test field background in Muonio. (a) Map of a selected part of the test field in Muonio. The blue dots show radar reflections produced by objects along the roadside. (b-d) Typical radar reflecting objects along the road. The objects include a parked car, several street signs and snow poles. The pictures are screenshots made from the RD CamLink – system. (e) Mean RCS values (Mean ± SD (SEM)) measured for the different objects. The values shown in the table are measured at 80 km/h in direction 1.

Further, different objects along the roadside were detected at different vehicle speeds. Selected were 30 km/h (similar to former test cases in Rovaniemi), 80 km/h (maximum speed allowed on the test track during the wintertime), and 60 km/h. **Figure 20a** shows the test results for a distance table. The results indicate that higher vehicle speeds lead to lower detected RCS values. The RCS-time plot shows, that at higher speeds, peak values were less frequently detected. This leads to lower RCS mean values and especially in the near range area to smaller standard deviations at higher speeds. Near range area means longitudinal distances up to 70 m. The lower graph in **Figure 20a** shows the time evolution of the RCS while the vehicle drove along the road. The oscillation of the RCS is based on its angle dependency. While driving, the angle between the radar and the reflector naturally changed due to the shifting path. **Figure 20b** shows the corresponding longitudinal distance – time plot of the radar reflections, caused by the distance table, while the vehicle drove along the road. The figure demonstrates that the distance table is always detectable in the near and far range area. In the far range area, the radar lost the connection to the distance table for 2 s (v = 30 km/h). During these 2 s the sightline between vehicle and table was blocked by a truck. Similar results were obtained from a bus stop (**Figure 20c**).

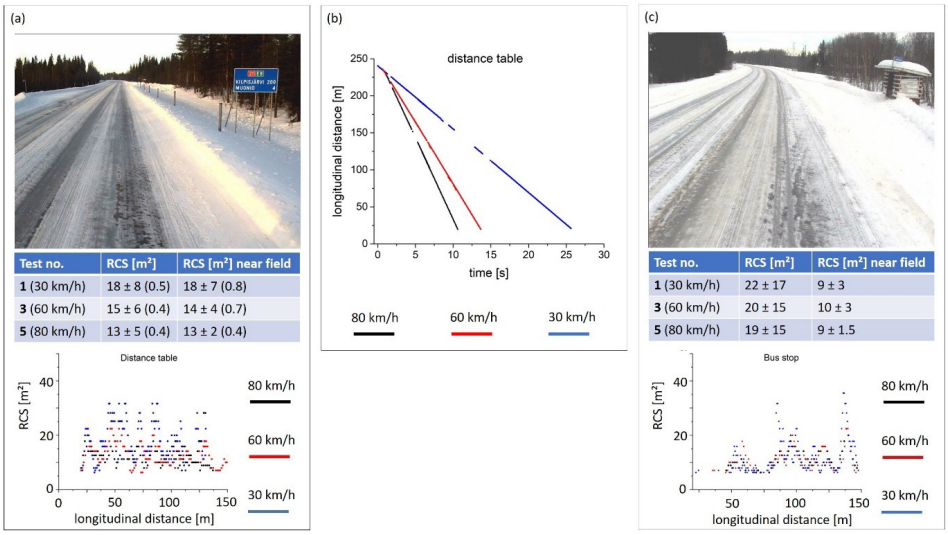

Figure 20: Test field background in Muonio measured with different vehicle speeds.(a) Mean RCS values measured for a distance table at different speeds (table). The values shown in the table are measured in direction 1. The values are shown in the form: Mean ± SD (SEM). The picture is a screenshot made with the RD CamLink – system. The lower graph shows the time evolution of the RCS for the distance table while the vehicle drove along the road. (b) Corresponding longitudinal distance – time plot of the distance table (near and far range area). (c) Time evolution and mean values of the RCS (Mean ± SD) measured for a bus stop at different speeds. The values shown in the table are measured in direction 1.

4.2.2 The Test Field with Reflector Poles

Based on the results obtained in **chapter 4.1**, mobile experiments with the test vehicle were performed on the test track in Muonio. Prior to the experiments, the 1.5 km long test track was prepared as described in **chapter 3.1**. The test track includes 97 self-designed tubular reflector poles on the left and right side of the road (pairwise in most cases). **Figure 21a** demonstrates a section of the test field in Muonio including the reflector poles. The Map shown in **Figure 21a** is from the "National Land Survey of Finland" WMS server. The presented radar reflection points in the Map (blue dots) were calculated using the distance and the offset provided by the radar as well as the GPS-position provided by the GPS and the IMU connected to the Lidar. Due to GPS and IMU not being connected directly to the radar, small positioning errors were introduced by the set-up, especially at longer distances.

Figure 21b shows a longitudinal distance-time plot including all 97 reflectors simultaneously. The data was produced while our test vehicle drove through the test field at 80 km/h in direction 1 (from south to north). The test was repeated under the same experimental conditions, but the test vehicle drove in direction 2 (**Figure 21c**). It should be noted, that most of the single linear graphs represent 2 reflector poles at the same longitudinal position (one on the left and one on the right side of the road). While measuring, the sensor from Continental was mounted on the front and the

cameras on the roof of the vehicle. The test field was continuously monitored with the radar while the vehicle drove.

The results show that, all 97 self-designed tubular reflector poles could be detected with a driving speed of 80 km/h. This result is particularly important because all previous tests in Rovaniemi (**chapter 4.1**) were carried out at a maximum speed of 30 km/h. Short losses of contact between individual reflectors and the radar are caused by other vehicles blocking the signal. It was further found, that reflector poles on the right side of the test vehicle send a stronger backscattered signal than corresponding poles on the left side of the car. The result can be explained by the fact, that poles on the left side of the car have a larger lateral distance from the radar than the corresponding pole on the right side. The measured RCS mean values (signal strengths) for the poles are $\sigma_{right} = (65 \pm 4{,}9)\ m^2$ and $\sigma_{left} = (49 \pm 3{,}3)\ m^2$. In comparison to other objects along the roadside (e.g. snow poles, signs), the detected RCS values of our self-designed reflector poles are, on average, two to three times larger. The data shows further smaller standard deviations for the detected RCS in the near range area compared to long distance measurements.

The green graph in **Figure 21b** shows reflector pair number 11. This reflector pair is analyzed in the next chapter.

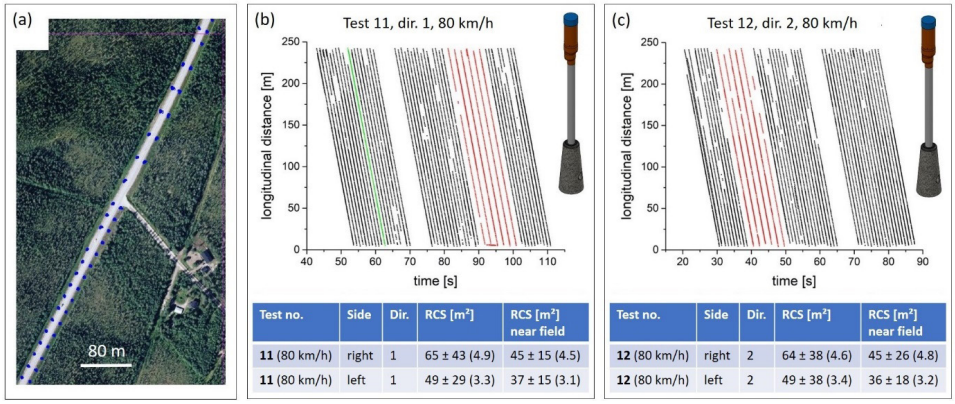

Test no.	Side	Dir.	RCS [m²]	RCS [m²] near field
11 (80 km/h)	right	1	65 ± 43 (4.9)	45 ± 15 (4.5)
11 (80 km/h)	left	1	49 ± 29 (3.3)	37 ± 15 (3.1)

Test no.	Side	Dir.	RCS [m²]	RCS [m²] near field
12 (80 km/h)	right	2	64 ± 38 (4.6)	45 ± 26 (4.8)
12 (80 km/h)	left	2	49 ± 38 (3.4)	36 ± 18 (3.2)

Figure 21: Mobile test with 97 self-designed tubular reflectors. (a) Map of a selected part of the test field in Muonio. The blue dots show radar reflections produced by our self-designed tubular reflector poles on the left and on the right side of the road. The longitudinal distance between the reflector poles is 20 m in the lower part of the figure and 40 m in the upper part. (b) Longitudinal distance-time plot for all 97 reflectors simultaneously. Most of the linear graphs represent two reflectors (one on the left and one on the right side) respectively. The red graphs represent poles with a longitudinal distance of 40 m while the black graphs represent poles with a distance of 20 m. The green graph shows the reflector pair number 11. The lower table shows weighted mean RCS values measured for all 97 self-designed reflector poles (separated by left and right side). The values are shown in the form: Mean ± SD (SEM). (c) Same content as in (b) but the test vehicle drove through the setup from the opposite direction.

4.2.3 Influence of the Driving Speed on Positioning and RCS

Studying the influence of the test vehicles speed on positioning of our self-designed tubular reflectors is a further essential goal of this study. **Figure 22** shows a qualitative analysis of positioning for one individual reflector pole measured at v = 30 and 80 km/h respectively. The spreading of the radar reflection values was manually measured by using a selection tool. The selection tool (ruler) is a feature which is integrated in the Road Doctor software.

The data shows that the positioning of the reflector poles is more accurate at lower vehicle speeds. Moreover, the longitudinal distances between the vehicle and the detected reflector poles affects the accuracy of the positioning. The positioning of a pole in the near range area, that means at longitudinal distances between 0 and 70 m, is on average more accurate than in the far range area. The measured data are in good accordance with [23].

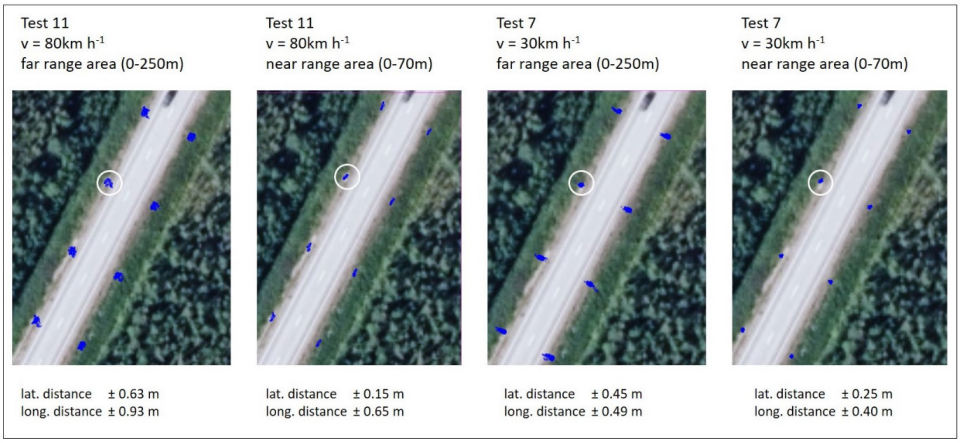

Figure 22: Influence of the driving speed on positioning. Map of a selected part of the test field in Muonio. The blue dots show radar reflections produced by our self-designed tubular reflector poles on the left and on the right side of the road. The longitudinal distance between the reflector poles is 20 m.

Further, one individual self-designed reflector pole (**Figure 8b**) was detected at different vehicle speeds. Selected were 30 km/h (similar to former test cases in Rovaniemi), 80 km/h (maximum speed allowed on the test track during the wintertime) and 60 km/h. **Figure 23** shows the test results for the representative pole pair. **Figure 23a** shows the longitudinal distance – time plot of radar reflections, caused by the selected pole, while the vehicle drove along the road. The reflector was on the right side of the test vehicle which drove in direction 1. **Figure 23c** shows the same experimental setup as in **Figure 23a** but the test vehicle drove in direction 2. Both figures demonstrate that the pole is well detectable at all tested speeds in the near and far range area. **Figure 23b** and **23d** show the corresponding RCS – longitudinal distance plots. The oscillation of the RCS values is based on the continuous change of the angle

between radar and reflector pole while the vehicle moved. Both, figures show, that at higher speeds, peak values are no longer detected. This leads to lower detected RCS mean values. The tables in **Figure 23e** and **23f** summarize the corresponding RCS mean values (signal strengths) for the single pole measured with different driving speeds. The measured RCS mean values for the pole pair are $\sigma_{dir1} = (79 \pm 6)$ m² and $\sigma_{dir2} = (81 \pm 4)$ m² and thus four times larger than the detected objects along the road-side (see chapter **4.2.1**).

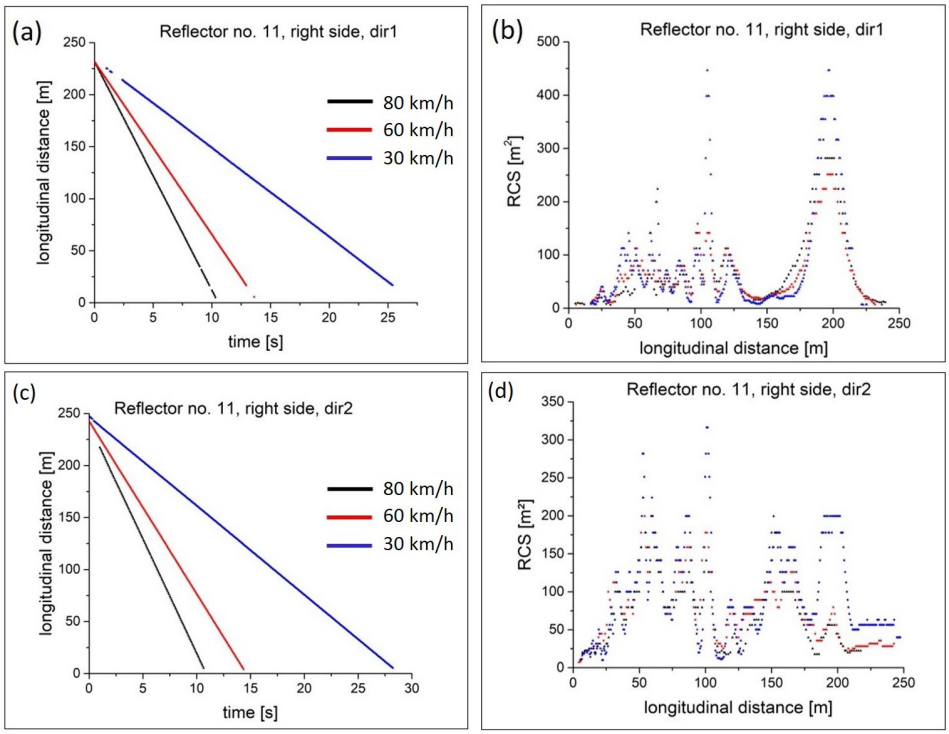

(e)

Test no.	Side	Direction	RCS [m²]	RCS [m²] near range
11 (80 km/h)	right	1	73 ± 73 (6.2) 65 ± 56 (5.0)*	30 ± 22 (3.6) 29 ± 18 (3.2)*
09 (60 km/h)	right	1	72 ± 59 (4.5) 65 ± 46 (3.6)*	49 ± 29 (4.4) 47 ± 26 (4.1)*
07 (30 km/h)	right	1	93 ± 107 (6) 80 ± 82 (4.9)*	66 ± 47 (5.2) 62 ± 37 (4.3)*

*5-95% intervall RCS: mean ± SD (SEM)

(f)

Test no.	Side	Direction	RCS [m²]	RCS [m²] near range
12 (80 km/h)	right	2	72 ± 47 (4.2) 69 ± 38 (3.6)*	82 ± 55 (8.8) 79 ± 47 (7.9)*
10 (60 km/h)	right	2	76 ± 46 (3.3) 73 ± 38 (2.9)*	91 ± 57 (7.9) 88 ± 48 (6.9)*
08 (30 km/h)	right	2	96 ± 61 (3.2) 93 ± 50 (2.7)*	87 ± 63 (6.3) 82 ± 51 (5.3)*

*5-95% intervall RCS: mean ± SD (SEM)

Figure 23: Influence of the driving speed on the RCS. (a) Longitudinal distance-time plot for one individual reflector (number 11) measured at different driving speeds. The reflector was on the right side of the test vehicle which drove in direction 1. (b) Corresponding RCS-longitudinal distance plot for reflector number 11. (c-d) Same experiment as in (a) and (b) but the test vehicle drove in direction 2. (e-f) Corresponding mean RCS values measured for reflector pole number 11 at three different speeds.

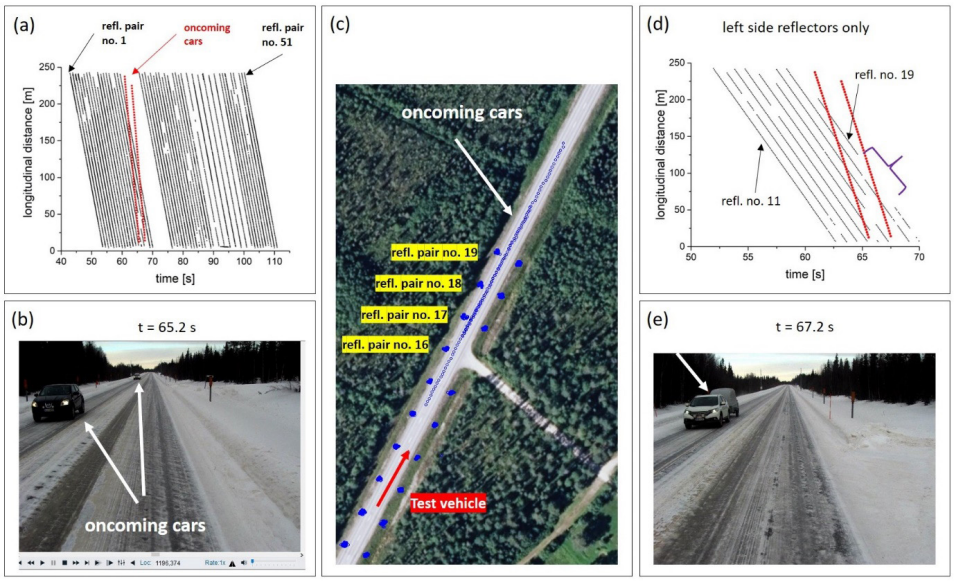

Figure 24: Two oncoming cars. (Test 11, dir1, v = 80 km/h). (a) Longitudinal distance-time plot for all 97 reflectors simultaneously (black linear graphs). The two linear graphs coloured in red show two oncoming cars. (b) Screenshot made with the RD CamLink – system of the two oncoming cars. (c) Map of a selected part of the test field in Muonio. The blue dots show radar reflections produced by our self-designed tubular reflector poles on the left and on the right side of the road. The longitudinal distance between the reflector poles is 20 m. The blue line in the center of the road represents radar reflections produced by the two oncoming cars. The red arrow shows the driving direction of the test vehicle. (d) Longitudinal distance-time plot for nine selected reflectors simultaneously (black linear graphs). The nine linear graphs represent radar reflections produced by the reflector poles on the left side of the road only. The two linear graphs coloured in red show two oncoming cars. The purple brace shows the situation, in which reflector pair number 19 (left side only) was blocked by the trailer of the second car. (e) The trailer of a car blocks the sightline to the reflector pole.

4.2.4 Other Vehicles on the Test Field

In the following chapter, the effect of oncoming cars on the detectability of our self-designed tubular reflector poles will be discussed. **Figure 24a** shows a longitudinal distance-time plot including all 97 reflectors simultaneously. The data were produced while the test vehicle drove through the test field with 80 km/h in direction 1 (from south to north). It should be noted, that most of the single linear graphs represent 2 reflector poles at the same longitudinal position (one on the left and one on the right side of the road). While measuring, the sensor from Continental was mounted on the front and the cameras on the roof of the vehicle. The test field was continuously monitored with the radar while the vehicle drove. The two linear graphs coloured in red show two oncoming cars. The steeper slope of the oncoming cars (compared to the reflector poles) results from the higher relative speed between the oncoming car and our test vehicle. **Figure 24b** shows a screenshot made from the RD CamLink – system of the two oncoming cars. It should be noted, that due to the proper height of the

camera on the roof of the test vehicle, the first oncoming car did not block the sightline between camera and reflector pole at any time. **Figure 24c** demonstrates the corresponding section of the test field in Muonio including the reflector poles (National Land Survey of Finland). Beside the radar reflections produced by the reflector poles on the left and on the right side of the road (blue dots), further reflections caused by two oncoming cars on the road are clearly visible. **Figure 24d** shows a zoom-in of **Figure 24a** including nine reflector poles on the left side of the test vehicle only. It can be seen, that the radar lost the connection to reflector number 19 for ≈ 3 s (purple brace). The result is shown in more detail in **Figure 25**. The reason for the contact loss is shown in **Figure 24e**. The trailer of the second car blocked the sightline between the camera and reflector pole. It can be assumed, that the trailer also blocked the signal between the radar and the reflector pole due to its position 60 cm above the ground.

The measured RCS mean values for oncoming cars are σ_{car1} = (86 ± 6,6) m² and σ_{car2} = (45 ± 2,2) m² and thus they are in the range of our self-designed reflector poles (**Figure 25**).

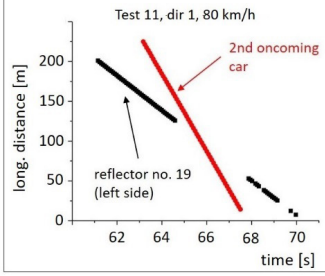

Test number	Oncoming car	Test vehicle direction	RCS [m²]	RCS [m²] near range
11 (80 km/h)	car 1, dir 2	1	98 ± 91 (11.4) 86 ± 50 (6.6)*	66 ± 50 (12.0) 64 ± 45 (11.5)*
11 (80 km/h)	car 2, dir 2	1	45 ± 20 (2.6) 45 ± 16 (2.2)*	27 ± 15 (3.6) 27 ± 13 (3.5)*
11 (80 km/h)	car 3, dir 2	1	19 ± 8 (1.0) 19 ± 7 (0.9)*	17 ± 6 (1.5) 17 ± 6 (1.5)*

*5-95% intervall
RCS: mean ± SD (SEM)

Figure 25: Oncoming car blocks the sightline to a reflector pole. Longitudinal distance-time plot for the left reflector of the pole pair number 19 (black linear graph) and an oncoming car (red linear graph). The gap in the black graph shows the situation in which the reflector was blocked by the trailer of the second car (left). Mean RCS values measured for three different cars at a driving speed of 80 km/h (right).

Finally, it can be stated, that oncoming cars can be detected by the 408-21 radar sensor from Continental up to 250 m longitudinal distance. Hereby the detected signal strength of the cars is in the range of our radar reflectors. Especially close oncoming cars with trailers can block the connection between the radar and the reflector poles on the left side of the road for 2 to 3 s (v = 80 km/h). In that case the pole on the right side is of essential importance. In the present tests, oncoming cars could not block the sightline between radar and reflector poles on the right and the left side of the road simultaneously.

4.2.5 Driving Behind a Truck – The Influence of Blowing Snow

Studying the influence of blowing snow on the detectability and the positioning of the self-designed reflector poles is an additional essential goal of the present study. For this purpose, a test-scenario was created, in which the test vehicle drove ≈ 30 m behind a truck. Due to the dry and cold weather conditions, the truck produced a trailing cloud of snow in which the test vehicle drove.

The photographs in **Figure 26a** and **26b** show screenshots made with the RD Cam-Link-system at two different point of times during the test. The number of seconds in the left upper side of the screenshots characterize the length of time elapsed since the test has started. The two diagrams in **Figure 26c** and **26d** show longitudinal distance-time plots for 49 reflectors simultaneously during the test drive (black linear graphs). The 49 black linear graphs represent radar reflections produced by the reflector poles on the right side of the road only. The green graph shows the truck in front of the test vehicle. The orange dashed line shows the position of the test vehicle while the corresponding screenshot was made. The two diagrams show further that, 55 seconds after the test has started, the test vehicle drove at a relatively constant distance of 30 m behind the truck.

The data shows that the self-designed reflector poles could be detected up to 250 m longitudinal distance under favorable conditions. Favorable condition means, that the truck did not totally block the sightline to the poles (**Figure 26a**). However, detecting reflector poles at ≈100 m or greater longitudinal distances was not possible most of the time due to signal obstruction (**Figure 26b**). Moreover, the truck itself is a strong radar multi-reflector. The truck, with an RCS of over 10000 m^2, is the strongest radar reflector which was detected during the whole study (**Figure 26e**). Another important finding is a decreased RCS mean value (signal strength) of the reflector poles compared to a test without the truck (**Figure 21c** and **26e**). The result indicates, that blowing snow weakens the detected RCS of the reflector poles.

Further, the influence of blowing snow on positioning of our self-designed tubular reflectors was investigated. **Figure 26f** and **26g** show a qualitative analysis of positioning for one individual reflector pole. The spreading of the radar reflection values was manually measured by using a selection tool. The selection tool (ruler) is a feature which is integrated in Road Doctor software. The data shows that the positioning of the reflector poles is less accurate if there is blowing snow between the reflector poles and the test vehicle (radar).

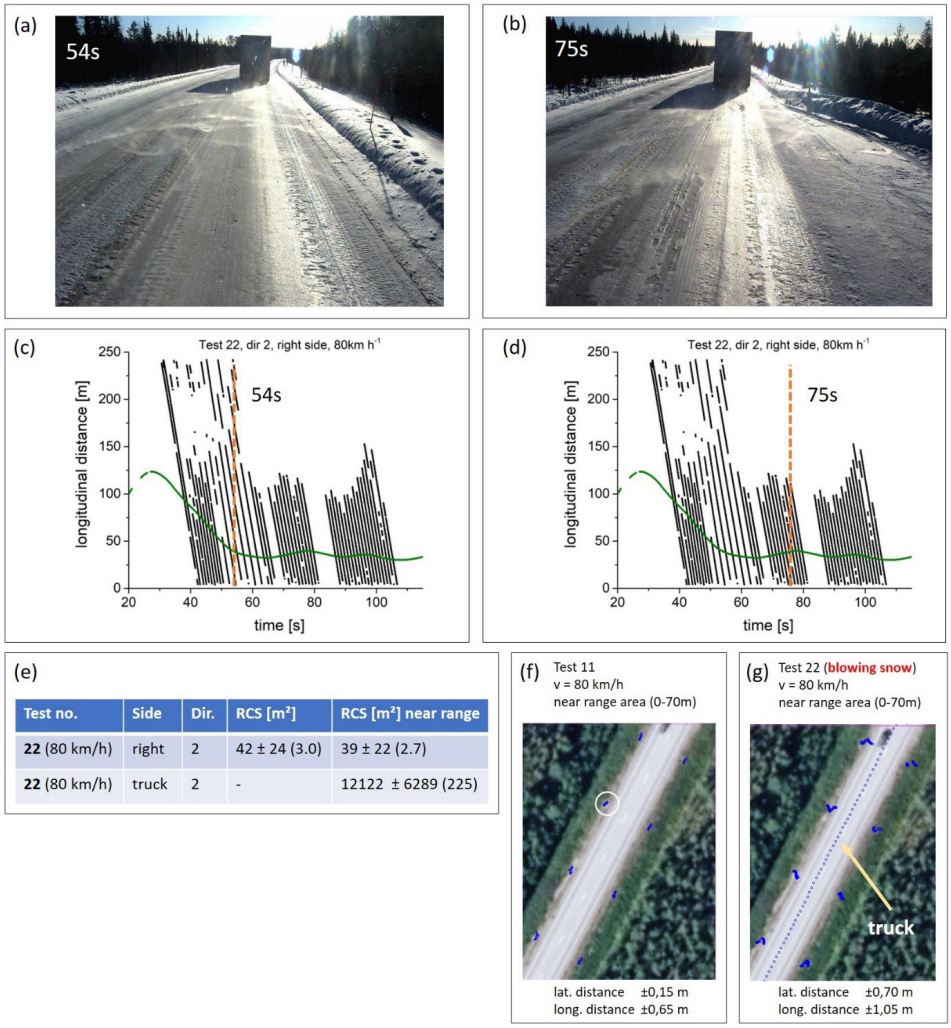

Test no.	Side	Dir.	RCS [m²]	RCS [m²] near range
22 (80 km/h)	right	2	42 ± 24 (3.0)	39 ± 22 (2.7)
22 (80 km/h)	truck	2	-	12122 ± 6289 (225)

Figure 26: Driving behind a truck. (a) Screenshot made with RD CamLink, 54 s after the measurement has started. (b) Screenshot made with RD CamLink, 75 s after the measurement has started. (c) Longitudinal distance-time plot for all reflectors on the right side simultaneously (black linear graphs). The green graph represents the truck. The orange dashed line shows the position of our test vehicle while the corresponding screenshot was made. (d) Longitudinal distance-time plot for all reflectors on the right side simultaneously (black linear graphs). The green graph represents the truck. The orange dashed line shows the position of our test vehicle while the screenshot was made. (e) Mean RCS values (mean ± SD (SEM)) measured for all 49 self-designed reflector poles (right side only) and the truck at a driving speed of ≈ 80 km/h. (f) Map of a selected part of the test field in Muonio. The blue dots show radar reflections produced by our self-designed tubular reflector poles on the left and on the right side of the road. The longitudinal distance between the reflector poles is 20 m. The test was performed without other cars in front of our test vehicle. (g) Same part of the road as in (f) but the test was performed while the test vehicle drove behind a truck.

5. Summary, Conclusion and Outlook

Autonomous driving could fundamentally revolutionise the automobile industry in the current century. Accurate detection of vehicles and other objects like physical land infrastructure is a challenging task for engineers and scientists. Radar systems and reflectors could play a key role in overcoming detection problems under harsh weather conditions, such as falling snow and rain. Radars can operate in almost all outer conditions making them indispensable to technologies supporting autonomous transport (e.g. ACC) [9]. [8]

To fully utilize the potential of radar systems for automotive applications under cold and icy road conditions, a research study that focuses on investigating passive roadside radar reflectors has been conducted. The present report contributes to a better understanding of prospects and limitations of current products in the field of automated vehicles with a focus on radar systems and radar reflectors. [8]

Chapter 2 of this report summarizes physical background information concerning radar systems and radar reflectors as well as laser scanning. **In chapter 3**, the radar system from Continental AG is introduced. This system is suitable for transport applications and was the foundation on which the field tests described in **chapter 4** were built. Moreover, four passive radar reflectors from the maritime sector and four self-designed corner reflectors are introduced. Based on previous test results of these self-designed reflectors, a tubular reflector pole was designed, developed further and produced.

Chapter 4.1 summarizes the practical field tests carried out during the winter period 2017/18. All results presented in **chapter 4.1** are published and discussed in [8]. Tested were three radar systems suitable for transport applications. Hereby, the radar from Continental performed best for our future applications concerning accuracy, resolution, data output and handling. Further, different types of passive radar reflectors (commercially used and self-designed) in different form and size were tested. The results indicate, that our self-designed Ø20 cm corner reflectors are a practicable, cheap and easy-to-produce alternative for our purposes compared to current products on the market. Based on these results, a tubular reflector pole was designed and an experimental setup on a road was developed.

Chapter 4.2 describes field tests carried out in Muonio during the winter period 2018/19. Studying the self-designed reflector pole on a road was the focus of these experiments. In **chapter 4.2.1** the test field background without reflector poles was studied. The characterization of objects along the road, such as roadside furniture, was the prior goal of this measurement. The surroundings of the road are characterized by multiple radar reflections. These reflections are caused by, among other things road signs, bus stops, big trees and house roofs. The road itself is free of radar reflections. Further, different objects along the roadside were detected at different vehicle speeds. The results indicate that higher vehicle speeds lead to lower detected RCS values. In **chapter 4.2.2** the test field including 97 self-designed tubular reflector poles was monitored with our test vehicle. The test should clear up, if and how well the poles are detectable by radar at a driving speed of 80 km/h. The results show that, all 97 self-designed tubular reflector poles could be detected with a driving speed of 80 km/h. This result is particularly important because all the previous tests discussed in **chapter 4.1** were performed with a maximum speed of 30 km/h. It was further found, that reflector poles on the right side of the test vehicle send a stronger backscattered signal than corresponding poles on the left side of the car. The result can be explained by the fact, that poles on the left side of the car have a larger lateral distance from the radar than the corresponding pole on the right side. The measured RCS mean values (signal strengths) for the poles are $\sigma_{right} = (65 \pm 4{,}9)\ m^2$ and $\sigma_{left} = (49 \pm 3{,}3)\ m^2$. In comparison to other objects along the roadside (e.g. snow poles, signs), the detected RCS values of our self-designed reflector poles are on average two up to three times larger. The data show further smaller standard deviations for the detected RCS in the near range area compared to long distance measurements. **Chapter 4.2.3** focusses on the influence of the driving speed on the positioning and the detected signal strength of the reflector poles. The data shows that the positioning of the reflector poles is more accurate at lower vehicle driving speeds. Moreover, the longitudinal distances between the vehicle and the detected reflector poles affects the accuracy of the positioning. The positioning of a pole in the near range area, that means at longitudinal distances between 0 and 70 m, is on average more accurate than in the far range area. The measured data are in good accordance with [23].

Moreover, the results show, that the self-designed reflector poles are well detectable at all tested speeds in the near and far range area. At higher speeds, peak values in the RCS were no longer detected. This leads to lower detected RCS mean values. The effect of oncoming cars on the detectability of the reflector poles are studied in **chapter 4.2.4**. The results show, that oncoming cars can be detected by the radar sensor from Continental up to 250 m longitudinal distance. Herby the detected signal strength of the cars is in the range of our radar reflectors. Especially close oncoming cars with trailers can block the connection between the radar and the reflector poles on the left side of the road for 2 to 3 s (v = 80 km/h). In that case the pole on the right side is of essential importance. Oncoming cars could not block the sightline between radar and reflector poles on the right and the left side of the road simultaneously. Finally, the influence of blowing snow on the detectability and the positioning of the self-designed

reflector poles is discussed in **chapter 4.2.5**. The results indicate, that blowing snow weakens the detected RCS of the reflector poles. The data further shows that the positioning of the reflector poles is less accurate if there is blowing snow between the reflector poles and the test vehicle (radar). Another result is that, under unfavorable conditions, a big truck in front of the test vehicle can obstruct the signal between the radar and those reflector poles which are further away than the truck. The pole interval that we selected (20 m) has proven to be advantageous, because at a driving speed of 80 km/h, a safe trailing distance between 2 vehicles should be at least 44 m. Consequently, if the truck blocked the signal between our test vehicle and the reflector poles, at least two reflector poles per side were always within the safe trailing distance, and thus detectable.

Finally, it can be stated, that the present study contributes to the understanding of prospects and limitations of current technologies and products in the field of autonomous driving with a focus on radars and passive reflectors. The present feasibility study should also act as a base for a future commercial application of the developed reflector poles. The results give a positive prognosis for developing the radar reflectors further and to scale their size smaller for more practical and cost-effective solutions. Smaller reflector diameters (≈11 cm) would open the possibility to include the reflectors in one single pipe instead of using a more complex geometry as presented in current study. Smaller size of reflectors could be compensated by adding more of them inside the pipe. Instead of having 3 there could be 9 or even more. Our self-designed reflector poles in combination with night reflectors would further support driving in bad environmental conditions such as darkness or fog.

Bibliography

REFERENCES

1. Stetter R, Witczak M and Pazera M 2018 Virtual Diagnostic Sensors Design for an Automated Guided Vehicle Applied Sciences 8 702
2. Teoh E R and Kidd D G 2017 Rage against the machine? Google's self-driving cars versus human drivers Journal of safety research 63 57–60
3. Yin H and Berger C 2017 - 2017 When to use what data set for your self-driving car algorithm: An overview of publicly available driving datasets 2017 IEEE 20th International Conference on Intelligent Transportation Systems (ITSC) 2017 IEEE 20th International Conference on Intelligent Transportation Systems (ITSC) (Yokohama, 16.10.2017 - 19.10.2017) (IEEE) pp 1–8
4. Shabbir J and Anwer T 2018 Artificial Intelligence and its Role in Near Future
5. Rama Rao P V S, Gopi Krishna S, Vara Prasad J, Prasad S N V S, Prasad D S V V D and Niranjan K 2009 Geomagnetic storm effects on GPS based navigation Ann. Geophys. 27 2101–10
6. Karthik Ramasubramanian B G 2017 AWR1243 sensor: Highly integrated 76–81-GHz radar front-end for emerging ADAS applications http://www.ti.com/lit/wp/spyy003/spyy003.pdf (accessed 17 May 2018)
7. Händel C., Konttaniemi H., Autioniemi M. 2018 State-of-the-Art Review on Automotive Radars and Passive Radar Reflectors : Arctic Challenge research project Lapland University of Applied Sciences
8. Autioniemi M, Konttaniemi H and Händel C 2019 Detecting Passive Radar Reflectors for Automotive Applications: Aurora Arctic Challenge Field Tests in 2018 LAPLAND UAS PUBLICATIONS
9. Scherr S, Gottel B, Ayhan S, Bhutani A, Pauli M, Winkler W, Scheytt J C and Zwick T 2015 - 2015 Miniaturized 122 GHz ISM band FMCW radar with micrometer accuracy 2015 European Radar Conference (EuRAD) 2015 European Radar Conference (EuRAD) (Paris, France, 09.09.2015 - 11.09.2015) (IEEE) pp 277–80
10. Skolnik M I 1983 Introduction to radar systems (International student edition) 2nd edn (Auckland: McGraw-Hill)
11. Avinash Singh Yadav, Sanjiv Kumar 2016 A Review Paper on Radar System International Journal for Innovative Research in Science & Technology 45–7

12. Christian Wolff Overview of Radar Transmitter http://www.radartutorial.eu/08.transmitters/Radar%20Transmitter.en.html (accessed 16 May 2018)
13. Demtröder W 2013 Experimentalphysik 6th edn (Berlin, Heidelberg: Springer Spektrum)
14. Alexey Voronov, Johan Hultén, Johan Wedlin and Cristofer Englund Radar reflecting pavement markers for vehicle automation
15. Ananya jadhav 2018 Retro-Reflective Materials © Ananya jadhav https://www.egypt-business.com/ticker/details/1826-retro-reflection-materials/308404 (accessed 21 Oct 2019)
16. wdwd 2011 Winkelreflektor3: phasengleiche Reflexion durch gleiche Streckenlängen a+b+c=a‘+b‘+c‘ https://commons.wikimedia.org/wiki/File:Winkelreflektor3.svg (accessed 23 May 2018)
17. Ronald Muellerschoen Instrument: Rosamond Calibration Array https://uavsar.jpl.nasa.gov/cgi-bin/calibration.pl (accessed 21 Oct 2019)
18. Armin W. Doerry and Billy C. Brock 2009 Radar Cross Section of Triangular Trihedral Reflector with Extended Bottom Plate: SANDIA REPORT http://prod.sandia.gov/techlib/access-control.cgi/2009/092993.pdf (accessed 23 May 2018)
19. Osman T I 2014 Analysis of Radar Cross Sectional Area of Corner Reflectors IOSRJEN 04 47–51
20. Marshall G F 2004 Handbook of Optical and Laser Scanning (Optical Science and Engineering) 2nd edn (Boca Raton: CRC Press)
21. Google LLC 2018 https://www.google.fi/maps/place/66%C2%B032’52.0%22N+25%C2%B048’36.0%22E/@66.5477778,25.81,439m/data=!3m1!1e3!4m5!3m4!1s0x0:0x0!8m2!3d66.5477778!4d25.81 (accessed 17 May 2018)
22. Roland Liebske 2016 ARS 404-21 Entry and ARS 408-21 Premium - Short Description: Technical Data http://www.compotrade.ru/i/pdf/ARS404-21_ARS408-21_en_V1.03.pdf (accessed 1 Jun 2018)
23. Continental AG 2017 ARS 408-21 Premium Long Range Radar Sensor 77 GHz https://www.continental-automotive.com/getattachment/5430d956-1ed7-464b-afa3-cd9cdc98ad63/ARS408-21_datasheet_en_170707_V07.pdf.pdf (accessed 24 May 2018)
24. Condon, Edward J and Kolbe, Edward and others (ed) 1978 Radar reflectors for boats (Marine electronics A28 no. 41)
25. Luke S 2007 Performance investigation of marine radar reflectors on the market.

LIST OF FIGURES AND TABLES

LIST OF ABBREVIATIONS

ACC	Adaptive Cruise Control
CAN	Controller Area Network
CW	continuous wave
DMI	Desktop Management Interface
FFT	fast Fourier transformation
FMCW	frequency modulated continuous wave
FTA	Finnish Transport Agency
GPR	ground penetrating radar
IF	intermediate frequency
Lidar	light detection and ranging
PLC	programmable logic controller
PLL	phase-locked loop
RCS	radar cross section
TI	Texas Instruments
TraFi	Transport Safety Agency

This report has been developed in the Arctic Challenge research project. The Arctic Challenge research project is funded by the Finnish Transport Agency (FTA) and the Finnish Transport Safety Agency (TraFi). The project is part of the Aurora intelligent road project of the Finnish Transport Agency and the NordicWay2 project funded by the Connecting Europe Facility of the European Union. The testing weeks for the research project will take place on the 10-km-long test stretch of the Aurora Vt21 (E8) intelligent road section in the years 2017–2019. Furthermore, the project is part of the Traffic Lab cooperation. The contracting partners involved in the research project include Dynniq Finland Oy, Indagon Oy, Infotripla Oy, Lapland University of Applied Sciences Oy, Roadscanners Oy, Sensible 4 Oy and VTT Technical Research Centre of Finland Oy.

The main author of this report was Dr. Chris Händel from Roadscanners Oy. The contributors from Lapland University of Applied Sciences have been Mr. Heikki Konttaniemi and Mr. Matti Autioniemi. Project engineers Mr. Matti Autioniemi, Mr. Jori-Jaakko Niskanen, Mr. Kari Moilanen from Lapland UAS have performed practical field-testing and developed test equipment with the help of Ward Martens, a thesis student, from PLX University College in Belgium, together with Dr. Händel. The project has been technically steered by Dr. Timo Saarenketo, Mr. Pekka Maijala and Mr. Timo Saarenpää from Roadscanners Oy.

Authors would also like to acknowledge Ilkka Kotilainen, Reija Viinanen and Alina Koskela from the Finnish Transport Agency, and Anna Schirokoff from the Finnish Transport Safety Agency, for their valuable help and support and steering of the project.

Note: Arctic Challenge promotes open data policy. Data from Arctic Challenge tests is made available for third parties

Co-financed by the European Union
Connecting Europe Facility

ROADSCANNERS

aurora
snowbox.fi

TRAFICOM

VÄYLÄ
Finnish Transport Infrastructure Agency

LAPIN AMK
Lapland University of Applied Sciences

www.laplanduas.fi

ISBN 978-952-316-327-0